Stability of Polydihydrosilane Liquid Films on Solid Substrates

Takashi Masuda [a], Yasuo Matsuki [a,c], Tatsuya Shimoda [a,b]

[a] Japan Science and Technology Agency, ERATO, Shimoda Nano-Liquid Process Project, 2-13 Asahidai, Nomi, Ishikawa, 923-1211, Japan.

[b] School of Materials Science, Japan Advanced Institute of Science and Technology, 1-1 Asahidai, Nomi, Ishikawa, 923-1292, Japan.

[c] Yokkaichi Research Center, JSR Corporation, 100 Kawajiri-cho, Yokkaichi, Mie, 510-8552, Japan.

Corresponding author: Takashi Masuda
Japan Science and Technology Agency, ERATO, Shimoda Nano-Liquid Process Project,
2-13 Asahidai, Nomi, Ishikawa, 923-1211, Japan.
TEL +81-761-51-7781
FAX +81-761-51-7791
E-mail: masuda@ishikawa-sp.com

Abstract

The quality of polydihydrosilane liquid films is a key factor in the fabrication of solution-processed silicon films. This study investigates the stability of polydihydrosilane liquid films with a thickness L of ~40 nm on solid substrates by a comparison between the observed optical microscope images and the values of the Hamaker constant A_{ALS} for the air/liquid (polydihydrosilane)/solid substrate systems. A_{ALS} values for a series of SiO_2-based substrates were determined by adopting a simple spectrum method. We found that the micrographs of the polydihydrosilane films provide direct evidence of stability in accordance with the sign of A_{ALS}; a stable liquid film with $A_{ALS} > 0$ showed a continuous figure, while an unstable film with $A_{ALS} < 0$ exhibited an array of dots caused by the rupture of the film. The array of dots in the unstable liquid films has a slight orderly distribution with a period λ that is in accord with the characteristic wavelength of the undulation related to the spinodal-like decomposition in van der Waals unstable liquid.

Keywords: liquid film, polysilane, polydihydrosilane, van der Waals energy, Hamaker constant

1. Introduction

Currently, silicon is the most widely used semiconductor material in electronic devices. Thin-film deposition techniques based on conventional vacuum processes, such as chemical vapour deposition and sputtering, are vital to modern industry. However, today, solution processes have attracted attention because of their wide application and cost-effectiveness in comparison to vacuum processes. We have demonstrated that a good-quality polysilicon film can be formed from a silicon precursor solution containing cyclopentasilane (CPS: Si_5H_{10}) and polydihydrosilane ($-(SiH_2)_n-$) dissolved in toluene [1]. For solution processes, basic properties, such as surface tension, polymer characteristics and the stability of the liquid film on the substrate, should be examined. We have clarified that the surface tension of CPS can be estimated on the basis of van der Waals interactions [2].

The solution-processed silicon film was fabricated by heating a polydihydrosilane liquid film with a thickness of several tens of nm coated on a solid substrate [1]. The liquid polymer film was transformed into a solid silicon film on heating. In that thickness region, van der Waals energy dominates the free energy of a liquid film and determines the film stability; thus, the stability of the liquid film may affect the uniformity of the resultant solid silicon film. Indeed, it was recognized that surface roughness of silicon films was observed after heating because of the non-uniformity of the liquid film coated on the substrates [1]. A detailed investigation of the liquid film stability is necessary to achieve a uniform and defect-free Si film.

The present study investigates the stability of polydihydrosilane liquid films on solid substrates by a comparison between the observed micrographs at room temperature and the calculated values of the Hamaker constant (A_{ALS}) for the air/liquid/solid substrate (*ALS*) systems. To efficiently compare the observations and A_{ALS} values, we selected five types of SiO_2-based substrates (quartz, glass and optical glasses A, B and C) and a TiO_2 substrate, because SiO_2 is a popular substrate for silicon devices. Since an evaluation of the Hamaker constant is essential for determining the stability of polymer films, we adopted a Simple Spectrum Method (SSM) [3,4] that is adequate for a system composed of materials with different resonance frequencies, such as solids and liquids. For comparison, we also calculated the A_{ALS} values based on the Tabor–Winterton approximation (TWA) [5]. We measured the optical parameters of several substances by an Abbe refractometer, ellipsometry and Fourier-transform infrared spectroscopy (FT-IR) to determine the optical parameters that appear in the London-dispersion (LD) spectra for the SSM.

2. Experiment

2.1 Polymer preparation

The liquid material consisted of a gelled polydihydrosilane synthesized by the photoinduced ring-opening polymerization of CPS. CPS was produced by the Kipping method [6,7]. It was placed in a square quartz cell and mixed using a stirrer while being irradiated with ultraviolet (UV) light (LAX–101; Asahi Spectra Co. Ltd). The wavelength, intensity and irradiation time were 365 nm, 1 mW/cm^2 and 60 min, respectively. By size-exclusion chromatography, we confirmed that CPS polymerized completely to polydihydrosilane under the above conditions.

2.2 Preparation of substrates and determination of optical parameters

The substrates quartz, glass, optical glasses A, B and C and TiO_2 used were 4 inches in size. The quartz was VIOSIL (Shin-Etsu Chemical Co. Ltd), the glass was OA-10 (Asahi Glass Company), the optical glasses A, B and

C were K-PSFn1.65, K-PSFn1.84 and K-PSFn2.14, respectively (Sumita Optical Glass, Inc.). TiO_2 was sputtered on OA-10. To use substrates with similar compositions minimizes the chemical influence of the substrate on film stability. The root-mean-square roughness of the surface for all substrates measured by scanning-probe microscopy (SPM) (SPM-3800; Seiko Instruments Inc.) was less than 0.3 nm. These substrates were ultrasonically cleaned using acetone, isopropyl alcohol and pure water for 10 min for each solvent, and then further cleaned by UV–ozone treatment for 15 min. Spin-coating was performed immediately after cleaning. The contact angle of the solution was under the measurable limit (5 degrees). In addition, the optical parameters of several of the substrates were determined by an Abbe refractometer, ellipsometry and FT-IR to determine the parameters required for the LD spectra calculations. The optical parameters are listed in Table A of Appendix A.

2.3 Film preparation and observation

Polydihydrosilane with a broad molar mass distribution ($M_W = 10^2$–10^6 g/mol) was dissolved in cyclooctane at 1.5 wt %. The solution was filtered by 0.2-μm polytetrafluoroethylene filters (Whatman Inc.). The film was coated on the solid substrate by spin-coating at 2000 rpm for 30 s. The resultant film thickness was 40 ± 5 nm. All processes (polymer preparation, spin-coating and surface oxidation) were carried out in a glove box because polydihydrosilane can easily be ignited in air. The oxygen and dew point in the glove box were less than 0.5 ppm and −75 °C, respectively. First, the coated-liquid film was stabilized overnight at room temperature in the glove box; then, only the film surface was oxidized slowly to freeze the pattern in the film and deactivate it. The resulting film, which was regarded as a polydihydrosilane film covered by a thin SiO_2 layer, was taken out into the atmosphere, and the films were observed using an optical microscope (BX-51; Olympus) and SPM in the contact mode at room temperature with a silicon nitride cantilever.

3. Results

3.1 Stability of liquid films

Here we present the micrographs of the polydihydrosilane films and discuss their stability by comparing these images with the values of the Hamaker constants.

Observations of liquid films

Figs. 1(a)–(f) show the micrographs of the polydihydrosilane films coated on six types of substrates (quartz, glass, optical glasses A, B and C and TiO_2). The A_{ALS} value calculated by the SSM based on Eq. (A.1) in Appendix A is noted on each image. Two types of prominent features—dot arrays and continuous figures—are observed in Figs. 1(a)–(f).

A large number of cyclic dots in the liquid films on the quartz (Fig. 1(a)) and glass substrates (Fig. 1(b)) indicate film rupture. The separations among the dots in the film on glass were slightly longer than those among the dots in the film on quartz. The film on the optical glass A showed two types of patterns: a patch-like configuration of dots in (c) and a continuous figure in (c'). In the present case, the two types of patterns coexisted in the same film. The images of the continuous films on optical glasses B and C and TiO_2 (Figs. 1(d)–(f)) were observed with high reproducibility.

The profile of a single dot in the array was measured by SPM. Fig. 2 shows the three-dimensional (3D) image by atomic force microscopy (AFM) for a typical dot on the glass substrate shown in Fig. 1 (b). The dot was shaped as a spherical cap with a height of 1.31 μm and a bottom diameter of 18.45 μm.

Hamaker constant

To quantify the liquid film stability observed in the micrographs of Fig. 1, we calculated the Hamaker constants based on the following model by the SSM (Appendix A) and the formula for the A_{ALS} from the TWA [5]. Fig. 3 illustrates the model of a liquid film with a thickness L coated on a solid substrate.

The stability of the liquid film is determined by the free-energy per unit volume $F(L) = \gamma_{SL} + \gamma_{LA} + P(L)$, where γ_{SL} and γ_{LA} are the interfacial energies of the solid/liquid and liquid/air boundaries, respectively, and $P(L)$ is the intermolecular interaction. When L is less than 1 μm, the energy term arising from gravity is ignored. For low-polarity materials, $P(L)$ is dominated by van der Waals energy: $P(L) = W_{ALS}(L)$ (see Appendix B). The W_{ALS} in the non-retarded Lifshitz theory [8, 9] is given by Eq. (1).

$$W_{ALS}(L) = \frac{A_{ALS}}{12\pi L^2} \quad (1)$$

According to this formula, a liquid film with $A_{ALS} > 0$ is stable, and that with $A_{ALS} < 0$ is unstable [10]. The A_{ALS} values in zJ unit obtained by the SSM (TWA) are −5.59 (–48.93), −1.43 (–36.43), 6.34 (–14.48), 13.81 (5.46), 29.28 (31.26) and 44.56 (60.65) for the liquid films on quartz, glass, optical glasses A, B and C and TiO_2 substrates, respectively. Furthermore, to examine the relationship between film stability and refractive index, the A_{ALS} values determined by the SSM (closed circles) and TWA (open squares) are plotted in Fig. 4 as a function of the refractive index of each substrate measured at 589 nm. The average value of the resonance frequency for the liquid material and substrate was used for the calculation of A_{ALS} in the TWA.

The results for both the SSM and TWA indicate that the liquid films on quartz and glass are unstable ($A_{ALS} <$ 0), and the liquid films on optical glasses B and C and TiO_2 are stable ($A_{ALS} > 0$). The TWA and SSM gave opposite signs for the A_{ALS} for the film on the optical glass A. Our observed micrographs are consistent with the stability of the liquid films determined by A_{ALS}, except for the film on the optical glass A. The stable films with $A_{ALS} > 0$ showed a continuous figure, while the unstable films with $A_{ALS} < 0$ showed an array of cyclic dots resulting from rupture. The observed image of the liquid film on the optical glass A showed a so-called metastable state caused by the appearance of both a continuous figure and a patch-like configuration of dots. It is quite intriguing that both stable ($A_{ALS} > 0$) and unstable liquid films ($A_{ALS} < 0$) appear for substrates consisting of SiO_2-based materials.

3.2 FFT analysis of dot arrays

The dot arrays appearing in the unstable films shown in Figs. 1(a) and (b) were analysed by the fast Fourier Transformation (FFT) algorithm to probe whether any periodicity exists. Fig. 5 shows one-dimensional (1D) FFT spectra of the film images on quartz and glass. The actual images of the 512 × 512 μm^2 areas of dots (Figs. 1(a) and 1(b)) and two-dimensional (2D) FFT spectra are shown in the upper right-hand side of each 1D FFT spectra in Fig. 5.

The highest peak of the 1D FFT spectra indicates the apparent existence of a non-random dot distribution, i.e. the dots have a slight orderly distribution with a period λ. The λ values estimated from the position of the highest peak (k_{max}) are $\lambda = 1/k_{max} \approx 53$ and 69 μm for the quartz and glass substrates, respectively. The peaks at higher wave numbers may be attributed to the dot diameters.

4. Discussion

4.1 Stability trends for the *ALS* system

Our main finding is the existence of a good correlation between the indication of stability, as observed in the micrograph images, and the sign of the A_{ALS} value calculated by the SSM. A question that needs to be addressed is the appearance of both stable ($A_{ALS} > 0$) and unstable liquid films ($A_{ALS} < 0$), despite the fact that nearly all substrates are SiO_2-based materials. The A_{ALS} value by the SSM [3,4] is calculated by considering the summation over the two variable s and ξ_n in Eq. (A.2) and Eq. (A.1) of Appendix A, respectively. By a simple estimation, it was found that $A_{ALS}(\xi_n)$ with $s = 1$ (named $A_{ALS}^{(1)}(\xi_n)$) in Eq. (A.2) dominates the summation of all s values. Therefore, we focused on the spectral features of $A_{ALS}^{(1)}(\xi_n)$ for three substrates (quartz, optical glasses A and C) to clarify the reason for the appearance of both the stable and unstable liquids in the present *ALS* system.

Figs. 6 (a) and (b) plot $A_{ALS}^{(1)}(\xi_n)$ versus ξ_n at $T = 293$ K for the liquid films on quartz, optical glass A and optical glass C and $\varepsilon(i\xi_n)$ versus ξ_n for the three substrates and polydihydrosilane using the Ninham–Parsegian model for $\varepsilon(i\xi_n)$ [3,11], respectively. The thin lines connecting the symbols are guides for the eye. From Fig. 6(a), we can understand that $A_{ALS} > 0$ for optical glass C, because $A_{ALS}^{(1)}(\xi_n) > 0$ for the entire frequency range of ξ_n. On the other hand, the sign of A_{ALS} for quartz and optical glass A is determined by Eq. (A.1) through a competition between $A_{ALS}^{(1)}(\xi_n) > 0$ and $A_{ALS}^{(1)}(\xi_n) < 0$, as seen in Fig. 6(a). Furthermore, it can be recognized in Figs. 6(a) and (b) that $A_{ALS}^{(1)}(\xi_n) > 0$ appears when $\varepsilon_S > \varepsilon_L$, while $A_{ALS}^{(1)}(\xi_n) < 0$ occurs when $\varepsilon_S < \varepsilon_L$. This difference is due to the fact that $A_{ALS}^{(1)}$ is proportional to $-\Delta_{AL}\Delta_{SL} \propto -(\varepsilon_A - \varepsilon_L)(\varepsilon_S - \varepsilon_L)$; thus, the sign of $A_{ALS}^{(1)}(\xi_n)$ is determined only by that of $\varepsilon_S - \varepsilon_L$, because $\varepsilon_A - \varepsilon_L < 0$ when $\varepsilon_A = 1$.

From the above simple analysis based on the $A_{ALS}^{(1)}(\xi_n)$ spectrum, it was clarified that the difference in the LD spectra between the liquid and substrate—$(\varepsilon_S - \varepsilon_L)$—determines the stability of the *ALS* system. The good correspondence between the observed images and A_{ALS} values obtained by the SSM arises from the appropriate description of $\varepsilon(i\xi_n)$ in the Ninham–Parsegian model. Through a more detailed investigation of ε_L and ε_S, it was found that the UV term in Eq. (A.4) (ω_{UV} and C_{UV} are listed in Table A is important to accurately describe the trend in stability for the present *ALS* system consisting of polydihydrosilane and SiO_2-based materials.

4.2 Possible origin of dot arrays in van der Waals unstable liquids

Our observation of dot arrays is quite interesting when considered in conjunction with the appearance of ruptured holes in other unstable polymer liquid films observed to date [12-14]. The ruptured holes were investigated as evidence of nucleation and dewetting. Kerle et al. [15] experimentally demonstrated that the non-random spatial distribution of holes originates from incipient undulation occurring the spinodal-like decomposition of van der Waals unstable liquids. In that case, the characteristic wavelength λ_{sp} of the incipient undulation was given by Eq. (2)

$$\lambda_{sp} = 4\pi L^2 \left(\frac{\pi \gamma_{LA}}{|A_{ALS}|} \right)^{1/2} \qquad (2)$$

Hence, if the spinodal-like decomposition occurred in the present polydihydrosilane liquid films, the slight orderly dot distribution with a period λ observed in Fig. 5 should be correlated to the distribution of the ruptured holes, i.e. $\lambda \approx \lambda_{sp}$. Before estimating λ_{sp} directly from Eq. (2), we speculated about the mechanism of the evolution from the ruptured holes to dot arrays associated with the spinodal-like decomposition [12,16]. The proposed mechanism begins with the appearance of an unstable capillary wave during the spinodal-like decomposition, as denoted by the dashed line in Fig. 7(a). When the amplitude of the unstable capillary wave equals film thickness, the unstable

mode leads to the rupture of the film, accompanied by the formation of the ruptured holes and the accumulation of polymer into the ridges of holes (solid line and arrows in Fig. 7(a), respectively). Furthermore, the accumulation of the polymer into the ridges is accelerated by the Rayleigh instability, and the polymer accumulated at the points of potential minima is transformed into a spherical cap in order to minimize the surface energy, as depicted schematically in Fig. 7(b).

If the mass of the polymer is brought together from the ruptured hole during the above evolution, the volume of the hole assuming a cylindrical form with a height L and a diameter λ should be equal to that of the observed spherical cap. The volume of the cylindrical hole on glass is 1.50×10^{-10} cm^3 with L = 40 nm and λ = 69 μm, while the volume of the spherical cap on the glass substrate in Fig. 2 is estimated to be 1.77×10^{-10} cm^3 with a height of 1.31 μm and a bottom diameter of 18.45 μm. This coincidence of volumes between them supports that the dot arrays are attributable to the droplets due to spinodal-like decomposition of unstable liquid. The λ_{sp} values obtained using Eq. (2) and A_{ALS} determined from the SSM (TWA) were 84 (26) and 167 (31) μm for the liquid films with L = 40 nm and γ_{LA} = 31.0 mN/m on the quartz and glass substrates, respectively. These results agree within an order of magnitude with the values of λ (53 and 69 μm, respectively) obtained by the FFT analysis.

Before concluding the present section, we suggest a way to synthesize a continuous Si film from an unstable liquid film by the solution process. If spinodal-like decomposition causes the instability of polydihydrosilane films, the fast solidification of a liquid film in less time than is needed for the growth of the ruptures should be effective. Therefore, rapid heating is important for achieving the above conditions, because the transformation from polydihydrosilane to an amorphous Si film occurs by heating. In addition, an increase in the growth time of the ruptures can be achieved by increasing L, viscosity η (high-molecular weight) and selecting substrates with low A_{ALS}, because the growth time for the mode with the maximum growth rate is given by $\tau_{max} = 48\pi^2\gamma_{LA}\eta L^5/|A_{ALS}|^2$ [17].

5. Conclusion

We have clarified the stability trends in polydihydrosilane liquid films of five types of SiO_2-based substrates (quartz, glass, optical glasses A, B and C) and a TiO_2 substrate by comparing the observed optical micrographs with the values of the Hamaker constant A_{ALS}. The micrographs of the liquid films depict two types of prominent features: a continuous figure and dot arrays, which are correlated to the stable and unstable liquid films, respectively, as determined by A_{ALS} calculated using the SSM. Through the SPM observation of a single dot, it was observed that the dot was shaped as a spherical cap. With regard to the dot arrays in the unstable films, the FFT analysis indicated a slight orderly distribution of the dots with a period λ. The fairly good agreement in the volume of the spherical caps and the cylindrical shaped holes, as well as in the length between λ and λ_{sp}, suggests that the dots observed for the quartz and glass substrates are attributable to the droplets originating from the ruptured holes that form because of the spinodal-like decomposition in van der Waals unstable liquids. The present results provide basic and important information for the fabrication of high-quality, solution-processed Si films from polydihyrosilane liquid films coated onto solid substrates.

Acknowledgment

This study was funded by the Exploratory Research for Advanced Technology (ERATO) program of the Japan Science and Technology Agency.

Appendix A: Hamaker constant

The Hamaker constant A_{ALS} was calculated by the SSM. The non-retarded form of A_{ALS} is written as Eq. (A.1) [3,4].

$$A_{ALS} = \sum_{n=0}^{\infty}{}' A_{ALS}(\xi_n) \qquad \text{(A.1)}$$

The prime on the summation in Eq. (A.1) indicates that the term of n = 0 is given half weight, and $\xi_n = n(2\pi k_B T/\hbar)$, where $\hbar$, k_B and T are Plank's constant, Boltzmann constant and the absolute temperature, respectively. The spectral component of A_{ALS} is given by Eq. (A.2)

$$A_{ALS}(\xi_n) = -\frac{3k_B T}{2}\sum_{s=1}^{\infty}\frac{(\Delta_{AL}\Delta_{SL})^s}{s^3} \qquad \text{(A.2)}$$

Δ_{kj} is the difference of the LD spectra defined in Eq. (A.3)

$$\Delta_{kj} = \frac{\varepsilon_k(i\xi_n) - \varepsilon_j(i\xi_n)}{\varepsilon_k(i\xi_n) + \varepsilon_j(i\xi_n)} \quad \text{(A.3)}$$

In Eq. (A.3), the LD spectra $\varepsilon(i\xi_n)$ are calculated from the imaginary part of the dielectric function $\varepsilon(\omega)$ by mathematical manipulation. The plot of $\varepsilon(i\xi_n)$ versus ξ_n is called the LD spectra. In the SSM, the modelled Ninham–Parsegian representation [12,4] for $\varepsilon(i\xi_n)$ is adopted, as in Eq. (A.4).

$$\varepsilon(i\xi_n) = 1 + \frac{C_{IR}}{1+(\xi_n/\omega_{IR})^2} + \frac{C_{UV}}{1+(\xi_n/\omega_{UV})^2} \quad \text{(A.4)}$$

$$C_i = \frac{2}{\pi}\frac{f_i}{\omega_i} \quad \text{(A.5)}$$

Thus, $\varepsilon(i\xi_n)$ is described by the parametric Lorentz oscillator model with a resonance frequency ω_i and an oscillator strength f_i. The indices (IR and UV) for ω_i and C_i represent the values in the infrared and ultraviolet regions, respectively. Since ω_{UV} and C_{UV} are important for the SSM, these values were determined by the Cauchy plot of refractive index measured using an Abbe refractometer and ellipsometry [2]. In addition, the ω_{IR} and C_{IR} values were obtained by FT-IR. We used the ω_{IR} and C_{IR} values for the quartz, glass and TiO_2 substrates reported in references [18-20]. The optical parameters ω_i and C_i (i = IR, UV) of our systems are listed in Table A. The A_{LAL}, A_{SAS} and A_{ALS} values estimated by (A.1) are also listed in Table A.

Appendix B: van der Waals and Acid–Base interactions

In a system with no electric double-layer effect, the intermolecular interactions $P(L)$ consist of the longer distance van der Waals interaction W^{vdW} (= $W_{ALS}(L)$) and the shorter distance acid–base (AB) interaction W^{AB}, as in Eq. (B.1). The latter is often called the hydrophobic interaction or hydration pressure [21].

$$P(L) = W^{vdW} + W^{AB} \qquad \text{(B.1)}$$

For a low-polarity material, the W^{AB} value is small. The W^{AB} values for materials 1 and 2 consist of the donor component γ^+ and the acceptor component γ^-, as in Eq. (B.2)

$$W_{12}^{AB} = 2\left[\sqrt{\gamma_1^+\gamma_2^-} + \sqrt{\gamma_1^-\gamma_2^+}\right] \qquad \text{(B.2)}$$

Explicit forms of γ^+ and γ^- are given in Ref. [21]. Associated with the molecular interaction, the surface energy γ is given by Eq. (B.3), with the vdW term γ^{vdW} and the AB term γ^{AB}.

$$\gamma = \gamma^{vdW} + \gamma^{AB}, \quad \text{(B.3)}$$

where

$$\gamma^{vdW} = \frac{A_{LAL}}{24\pi D_0^2} \quad \text{(B.4a)}$$

$$\gamma^{AB} = 2\sqrt{\gamma^+\gamma^-} \quad \text{(B.4b)}$$

In Eqs.(B.4a,b), D_0 denotes the cut-off distance that is adopted (0.165 nm) [9]. For a low-polarity material, the value of γ^{AB} is small. The measured surface energy (γ) of polydihydrosilane is 31.0 mN/m, and the calculated value for γ^{vdW} using Eq. (B.4a) is 33.1 mN/m. Consequently, $P(L)$ is mainly determined by van der Waals energy in the polydihydrosilane thin liquid film because of its low polarity nature ($\gamma \approx \gamma^{vdW}$, $\gamma^{AB} \approx 0$).

References

[1] T. Shimoda, Y. Matsuki, M. Furusawa, T. Aoki, I. Yudasaka, H. Tanaka, H. Iwasawa, D. Wang, M. Miyasaka, Y. Takeuchi, Nature 440 (2006) 783.

[2] T. Masuda, Y. Matsuki, T. Shimoda, J. Colloid Interface Sci. 340 (2009) 298.

[3] D.B. Hough, L.R. White, Adv. Colloid Interface Sci. 14 (1980) 3.

[4] R.H. French, J. Am. Ceram. Soc. 83(9) (2000) 2117.

[5] D. Tabor, R.H. Winterton, Proc. Roy. Soc. A. 312 (1969) 435.

[6] F.S. Kipping, J. Chem. Soc. 125 (1924) 2291.

[7] E. Hengge, G. Bauer, Angew. Chem. 85 (1973) 304.

[8] E.M. Lifshitz, Sov. Phys. JETP 2 (1956) 73.

[9] J.N. Israelachvili, Intermolecular and Surface Forces, 3rd ed., Academic Press, New York, 2010.

[10] A. Martin, O. Rossier, A. Buguin, P. Auroy, F. Brochard-Wyart, Eur. Phys. J. E 3 (2000) 337.

[11] B.W. Ninham, V.A. Parsegian, G.H. Weiss, J. Stat. Phys. 2 (1970) 323.

[12] A. Sharma, G. Reiter, J Colloid Interface Sci. 178 (1996) 383.

[13] T. Stange, D.F. Evans, W.A. Hendrickson, Langmuir 13 (1997) 4459.

[14] G. Reiter, Langmuir 9 (1993) 1344.

[15] T. Kerle, R. Yerushalmi-Rozen, J. Klein, L.J. Fetters, Europhys. Lett. 44(4) (1998) 484.

[16] V.S. Mitlin, J. Colloid Interface Sci. 156 (1993) 491.

[17] P.G. de Gennes, F. Brochard-Wyart, D. Quere, Capillarity and Wetting Phenomena: Drops, Bubbles, Pearls, Waves, Springer, New York, 2010.

[18] L. Bergstrom, Adv. Colloid Interface Sci. 70 (1997) 125.

[19] D.R. Lide, CRC Handbook of Chemistry and Physics, 88th ed., CRC Press, 2007.

[20] C.J. Pouchert, The Aldrich Library of FTIR Spectra, Aldrich Chemical Company, Inc, 1985.

[21] C.J.V. Oss, M.K. Chaudhury, R.J. Good, Chem. Rev. 88 (1988) 927.

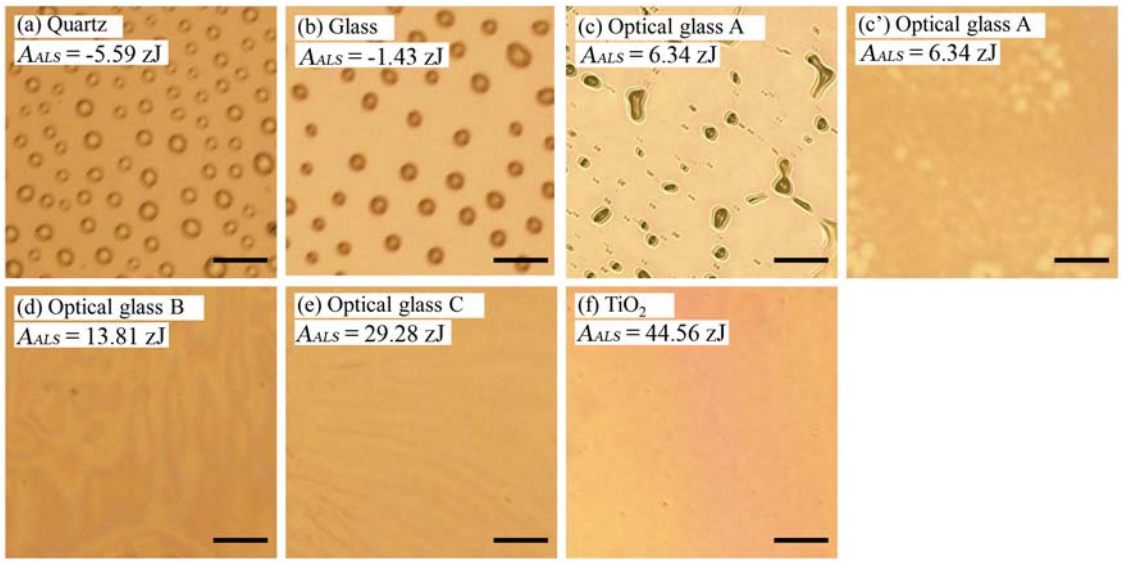

Fig. 1. Optical micrographs of polydihydrosilane films on different substrates: (a) quartz, (b) glass, (c,c') optical glass A, (d) optical glass B, (e) optical glass C and (f) TiO_2. The figures (c) and (c') display the images at different points on the same film. The A_{ALS} values calculated by the SSM is noted on each micrograph. The length of the bar in each image is 100 μm.

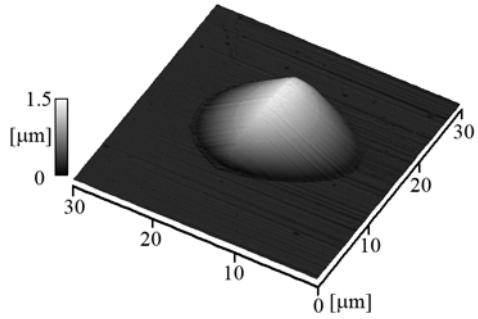

Fig. 2. AFM image of a single dot on the glass substrate in Fig. 1(b). The height and width of the dot are 1.31 and 18.45 μm, respectively.

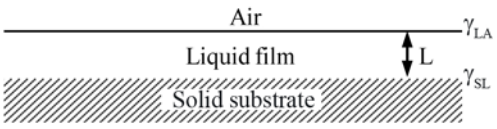

Fig. 3. Model of a liquid film on a solid substrate

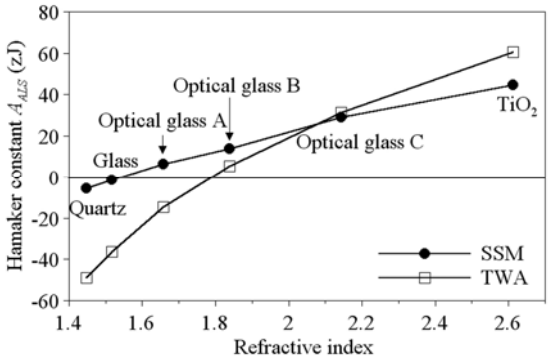

Fig. 4. A_{ALS} versus n (refractive index of the substrates measured at 589 nm)

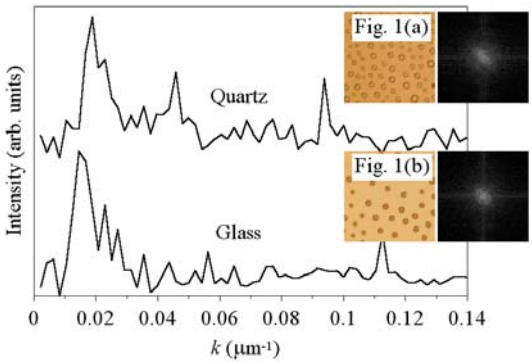

Fig.5. 1D and 2D FFT spectra for quartz and glass substrates. 1D FFT spectra were obtained from 2D FFT spectra. The actual images of the 512 × 512 μm^2 area (Figs. 1(a) and 1(b)) and 2D FFT spectra are shown in the upper right-hand side of the 1D FFT spectra. The sharp peaks in the 1D FFT spectra suggest a non-random dot distribution. The obtained periods are 53 and 69 μm for the quartz and glass substrates, respectively.

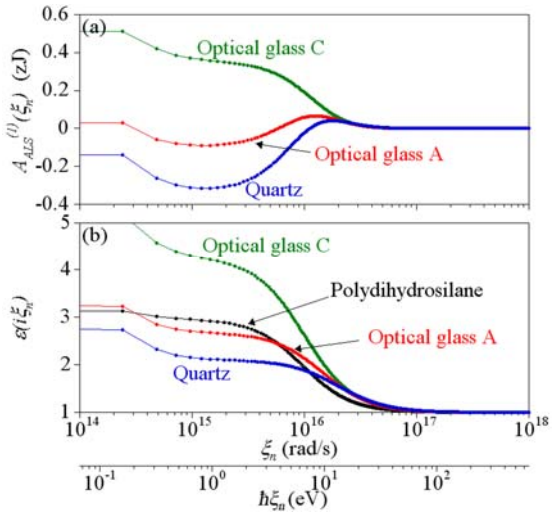

Fig. 6. (a) $A_{ALS}^{(1)}(\xi_n)$ versus ξ_n for the liquid films on quartz, optical glasses A and C substrates. (b) $\varepsilon(i\xi_n)$ versus ξ_n (the LD spectra) for quartz, optical glasses A and C and polydihydrosilane. The second x-axis denotes the $\hbar\xi_n$ in eV for T = 293 K.

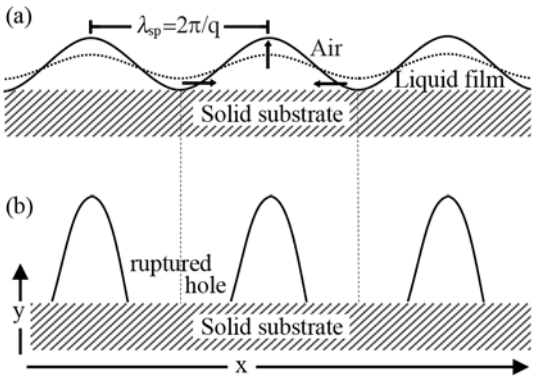

Fig. 7. Schematic of the unstable capillary wave mode, holes and dot arrays: (a) unstable mode with wavelength λ_{sp} (dashed line) during the spinodal-like decomposition, and the appearance of the ruptured holes with polymer accumulation (solid line). (b) dot arrays. Note that scales of the x and y-axes differ by a factor of ~ 5×10^3 in (a), while that factor in (b) is ~ 200.

Table A

Optical parameters and Hamaker constants

	C_{UV}	ω_{UV} (rad/s)	C_{IR}	ω_{IR} (rad/s)	A_{LAL} or A_{SAS} (zJ)	A_{ALS} (zJ)
Polydihydrosilane	1.96	9.71×10^{15}	0.54	1.66×10^{14}	–67.88	
SiO_2 (Quartz)	1.10	2.02×10^{16}	1.71	1.86×10^{14}	–65.03	–5.59
SiO_2 (Glass)	1.26	1.84×10^{16}	1.55	1.74×10^{14}	–71.71	–1.43
Optical glass A	1.67	1.46×10^{16}	1.80	1.61×10^{14}	–83.65	6.34
Optical glass B	2.20	1.17×10^{16}	1.90	1.76×10^{14}	–96.00	13.81
Optical glass C	3.23	1.00×10^{16}	2.08	2.20×10^{14}	–128.19	29.28
TiO_2	4.88	7.97×10^{15}	108	7.00×10^{14}	–159.87	44.56